Chapter 6
Composite Nanowires for Room-Temperature Mechanical and Electrical Bonding

Yanbin Cui and Yang Ju

Abstract At millimeter dimension or less, the conventional bonding technology in electronic assembly relies heavily on reflow soldering and suffers from severe performance and reliability degradation. Meanwhile, the traditional high temperature bonding process (easily reach 220 °C) tends to result in undesired thermal damage and residual stress at the bonding interface. It is therefore a major challenge to find a means to preparing room-temperature connectors or fasteners with good mechanical and electrical bonding. Very recently, composite nanowires have been used to fabricate room-temperature fasteners. In this chapter, we summarize the state-of-the-art progress on the use of composite nanowires for room-temperature mechanical and electrical bonding. Using anodic aluminum oxide (AAO) and polycarbonate (PC) membrane as templates, the fabrication of Cu/parylene and Cu/polystyrene nanowires was described, while the fabrication of carbon nanotube (CNTs) array used to connect with Cu/parylene nanowires was also introduced. Finally, the performances of the composite nanowires (Cu/parylene, Cu/polystyrene, and CNT-Cu/parylene) used as surface fastener for room-temperature mechanical and electrical bonding were demonstrated.

6.1 Introduction

Surface mount devices (SMDs) relies heavily on reflow soldering and has become the cornerstone of today's electronic industry. The heating temperatures of traditional reflow soldering technique can easily reach 220 °C during reflow soldering, which may not only cause energy consumption but also thermal damage to the

Y. Cui
State Key Laboratory of Multiphase Complex System, Institute of Process Engineering, Chinese Academy of Sciences, Beijing 100190, China
e-mail: ybcui@ipe.ac.cn

Y. Ju (✉)
Department of Mechanical Science and Engineering, Nagoya University, Nagoya 464-8603, Japan
e-mail: ju@mech.nagoya-u.ac.jp

S.A. Meguid (ed.), *Advances in Nanocomposites*,
DOI 10.1007/978-3-319-31662-8_6

surface mount components. Additionally, the toxicity of traditional Sn-Pb solder has led to a trend of worldwide legislation that mandates the removal of lead from electronics. Although various types of lead-free solder have been proposed and adopted in the electronics industry, the melting points of these lead-free solders are always 5–20 °C higher than Sn-Pb solder. Moreover, the recycling of rare metals in the surface mount components and printed circuit boards is not easy due to the difficulties in detaching the components, circuit boards, and solder materials (Ju et al. 2012). On the other hand, the continuous trend toward miniaturization and functional density enhancement makes it necessary to improve the bonding technology in surface mount technology (SMT). At millimeter dimensions or less, conventional electrical connectors or fasteners tend to suffer from severe performance and reliability degradation (Cui et al. 2014a). It is therefore a major challenge to find a nontoxic and room-temperature bonding technique that afford good mechanical bonding as well as electrical contact; especially for micro/nano-electronic circuits and flexible electronic devices.

With regard to developing a room-temperature bonding technique for SMT, one possible approach is to make use of cold welding. Cold welding of thin gold films on elastomeric supports has been carried out under ambient conditions and low loads (Ferguson et al. 1991). However, only the lower limit of approximately 0.1 N/cm^2 was reported for the adhesion strength. Besides, many researchers have also succeeded in joining individual nanostructures by nanoscale-welding method (Dong et al. 2006; Jin et al. 2008; Peng et al. 2008). Although direct heating was not performed and large forces were not applied in these nanoscale-welding techniques, fine manipulation of an individual nanowire or nanotube by specific equipment was always necessary. Therefore, these nanoscale-welding techniques, in which the connection between two nanowires or nanotubes was performed, are suitable for nanoscale connection but inefficient for the mass production of SMDs.

Recently, hybrid core/shell nanowire forests have been used to fabricate electrical and chemical connectors (Ko et al. 2009; Kapadia et al. 2009). Specifically, we prepared a serial of nanowire (including metallic and hybrid core/shell nanowire arrays) and carbon nanotube (CNT) arrays, in which the nanowire and CNT arrays were used as a fastener for SMT (Cui et al. 2014a, b; Ju et al. 2012; Teshima et al. 2014; Wang et al. 2013a, b, 2015). For SMT, the fastener should ideally have both high adhesion strength and provide a good electrical connection. In this chapter, we summarize the state of the art concerning the use of composite nanowires for room-temperature mechanical and electrical bonding. First, the fabrication of anodic aluminum oxide (AAO) membrane, which used for the growing Cu nanowires, is presented. Then, using AAO and polycarbonate (PC) membrane as templates, the synthesis of copper/parylene and copper/polystyrene composite nanowires are described and discussed. While, the fabrication of carbon nanotube (CNTs) array used to connect with Cu/parylene nanowires is also introduced. Lastly, the performances of the composite nanowires used as surface fastener for room-temperature mechanical and electrical bonding are demonstrated.

6.2 Fabrication of Anodic Aluminum Oxide Membrane

Anodic aluminum oxide (AAO) nanoporous membrane is popular for its self-organized nanostructure. Due to its highly ordered porous structure, significant thermal stability, and cost-effectiveness (Woo et al. 2005; Li et al. 2005), AAO membranes are widely used for the fabrication of nanowires and nanotube arrays to be utilized as filters, sensors, catalysts, and solar cells, among others (Woo et al. 2005; Gorokh et al. 2006; Attaluri et al. 2009; Wei et al. 2008; Zhiyong et al. 2009). Since Masuda and Fukuda (1995) introduced two-step anodization, the AAO got more attention from nanotechnology community. In order to produce highly ordered nanopore structures, a significant number of studies concerned with process parameters had been carried out. By changing the anodizing parameters (such as electrolytes, anodizing voltage, anodizing time, temperature, and etching methods), the structure of AAO (such as pore size, pore depth, interpore distance, thickness of membrane, and pore geometry) can be easily controlled (Crouse et al. 2000; Gâlcă et al. 2003; Chu et al. 2005; Kasi et al. 2012). AAO templates exhibit columnar pore structure, vertical to the substrate and parallel to each other with pore diameters from several tens to hundreds nanometers and with an aspect ratio between 10 and 1000 or more (Crouse et al. 2000; Chen et al. 2003; Pu et al. 2004). By filling the pores of the AAO templates, arrays of well-aligned nanowires or other 1D nanostructures with uniform diameter and length can be obtained using electroplating or other growth methods (Yan et al. 2007).

In general, a two-step anodization method was employed to produce well-arranged porous AAO template (Masuda and Fukuda 1995). Typical fabrication processes of the AAO template are shown in Fig. 6.1. Appropriate electrolyte solution (such as oxalic acid) was used for the anodization. The pretreated

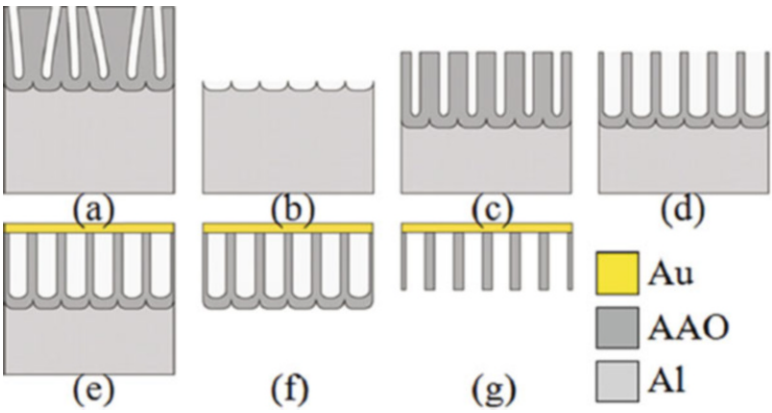

Fig. 6.1 Schematic of fabricating the AAO: (**a**) a first-step anodization, (**b**) wet etching of AAO fabricated in a first-step anodization, (**c**) a second-step anodization, (**d**) extending the pores, (**e**) sputtering Au film, (**f**) dissolving aluminum substrate, and (**g**) dissolving barrier layer and extending pores (Teshima et al. 2014)

aluminum foils were anodized in electrolyte solution under constant voltage at room temperature. At the first anodization step, the alumina layer fabricated was dissolved by wet chemical etching in a mixture of 6 wt% phosphoric acid and 1.5 wt% chromic acid solution for 30 min at 60 °C. The resulting inner aluminum foils have uniform concave nanoarray, which is crucial to achieving ordered pore size distribution (Belwalkar et al. 2008). After removal, the second anodization step was carried out at the same condition. After the two-step anodization process, the remaining aluminum on the AAO was dissolved in the solution made up of one part by volume of 0.1 mol/L $CuCl_2$ solution and four parts by volume of 10 wt% HCl (Belwalkar et al. 2008). Finally, the oxide barrier layer of the AAO was removed and the pores were enlarged by floating the sample on the surface of 0.5 mol/L phosphoric acid solution at room temperature using to the surface tension of the AAO (Cui et al. 2012).

It is well known that the value of the anodizing voltage for preparing the best nanopore order in self-ordered AAO is different for each electrolyte (Zaraska et al. 2011). For instance, in sulfuric acid, oxalic acid, and phosphoric acid, anodizing voltages were 25, 40, and 195 V, respectively. If a higher anodizing voltage is applied, then the higher current density and Joule heating generation will cause damage or lead to the collapse of the pore structure. In practice, a higher potential is beneficial in increasing the pore size. Chung et al. (2013) proposed a high-potential hybrid pulse anodization (HPA) technique to resolve this problem. In HPA technique, a period of small negative potential is applied to suppress the Joule heating effect during the AAO preparation process. The scanning electron microscope (SEM) results showed that HPA with an anodizing potential of 60 V resulted in an intact pore structure on the AAO surface (Fig. 6.2). By contrast, the AAO formed using conventional direct current anodization (DCA) with the same anodizing potential contained many small irregular pores around each original pore (Fig. 6.2a) (Chung et al. 2013). On the other hand, it is clearly seen that the reduction of the irregular small branch pores in AAO formed by HPA, as shown in Fig. 6.2b. Chung et al. (2011) also found that the HPA technique not only merits manufacturing convenience and cost reduction but also promotes pore distribution

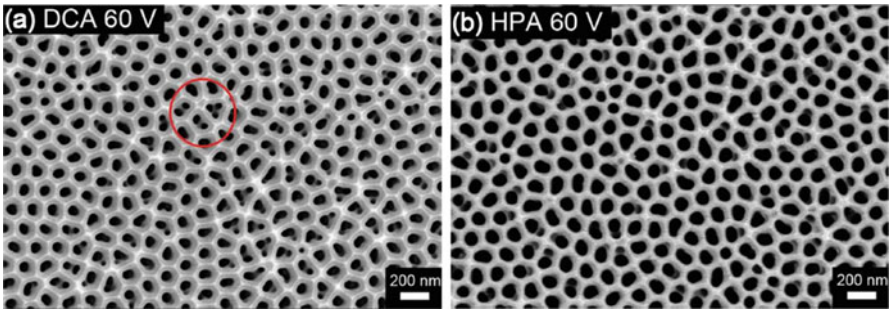

Fig. 6.2 Top-view SEM micrographs of AAO nanostructures formed by (**a**) DCA 60 V, (**b**) HPA 60 V with following pore widening for 10 min (Chung et al. 2013)

uniformity of AAO at severe conditions of low-purity Al foils and relatively high room temperature. The pore distribution uniformity can be improved by HPA compared with the DCA. Very good AAO distribution uniformity (91 %) was achieved in high-purity aluminum foil by HPA. This is because it can suppress the heating effect to diminish the dissolution reaction (Chung et al. 2011).

Controlling the size and uniformity of the pores is the key in manipulating the structure and properties of the materials confined within the pores of AAO. Kim et al. (2007) reported a new approach for preparing pretextured surface patterns on aluminum using solvent-dependent differential swelling of block copolymers. Long-range order in a hexagonal-packed monolayer was created using solvent-induced ordering of poly (styrene-b-4-vinylpyridine) (PS-b-P4VP) micellar films, followed by surface reconstruction to make nanoporous patterns. Using reactive ion etching (RIE), patterns were transferred to the Al surface. Subsequent anodization in concentrated sulfuric acid enabled the formation of channels with long-range lateral order. Highly ordered porous alumina with a hole interval of 45 nm and a hole size of 12 nm was produced (Fig. 6.3) (Kim et al. 2007).

Besides, ultrathin AAO membranes were also be used as masks for the fabrication of nanoparticle arrays on different surfaces. The AAO membranes can be formed directly on some surfaces, such as silicon and indium tin oxide. Typically, a thin layer of Al is deposited on these substrates, and nanoporous masks are fabricated by the anodization of this layer (Chu et al. 2001; Mao et al. 2009). Pastore et al. (2011) fabricated ultrathin AAO membranes by applying low anodization voltages that provide low reaction speed during AAO formation. A low anodization speed is required to obtain membrane thickness below 100 nm in a reproducible manner. With this procedure, AAO membranes with pore diameters below 20 nm and membrane thickness below 70 nm were obtained (Pastore et al. 2011).

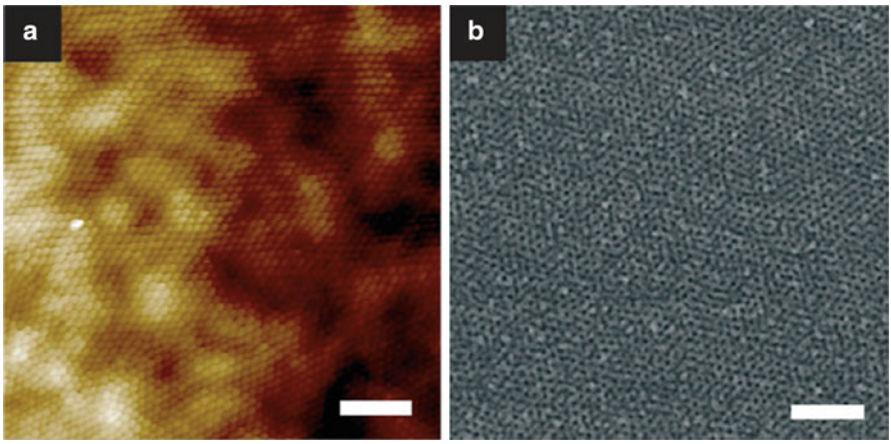

Fig. 6.3 Scanning force microscopy (SFM) image of surface view of anodized Al in 2.5 M sulfuric acid at 19 V at 48 °C for 10 min (**a**) and SEM image of anodized Al after pore widening carried out in 5 wt% phosphoric acid at 20 °C for 5 min (**b**). (Scale bar: 200 nm.) (Kim et al. 2007)

6.3 Synthesis of Copper/Parylene Composite Nanowires

Due to its ability to control nanomaterial shape, size, and uniformity, template-assisted synthesis has attracted considerable attention and proved to be a simple and versatile approach for preparing ordered nanowire, nanorod, nanoparticle, and nanodot arrays in a wide range of materials (Huczko 2000; Xu et al. 2010). Numerous nanomaterials have been prepared by utilizing hard templates such as track-etched polycarbonate (PC) membranes (Demoustier 2001), AAO templates (Ding et al. 2006; Wei et al. 2005), and soft templates such as polymers (Sumikura et al. 2008) and surfactants (Bakshi et al. 2007). On the other hand, various techniques, such as chemical vapor deposition (Venkatasubramanian et al. 2001), molecular beam epitaxy (Harman et al. 1999), vapor–liquid–solid growth process (Li et al. 2003), and hydrothermal process (Li et al. 2001), have been applied to synthesize nanowire- and/or nanotube-structured materials. Compared to those methods, electrodeposition is one the most cost-effective techniques to fabricate the nanostructured materials (Feng et al. 2008). Therefore, directional growth of nanowires/rods/pillars through PC or AAO templates via electrodeposition process is a very popular method because of its inexpensive, simple technique and ability to incorporate complex geometrical structures and easy tenability of the nanopores' dimensions (also nanowires/rods' dimension) by controlling the deposition parameters (Joo and Banerjee 2010).

Recently, Ge/parylene core/shell nanowire array was used as an electrical connector after the deposition of an Ag film with relatively high shear adhesion strength (Kapadia et al. 2009). In addition, Ni and Cu nanowire arrays have been found to have very low electrical resistance (Baek and Fearing 2009; Xu et al. 2012). Specially, nanowire surface fasteners based on gold and copper nanowire arrays were also proposed (Ju et al. 2012; Wang et al. 2013a), with relatively low electrical resistance and adhesion strengths. However, the maximum adhesion strength of the metallic nanowire surface fastener is only 8.17 N/cm^2. Therefore, it is still a challenge to achieve high adhesive strength and low electrical resistance at the same time for room-temperature surface fastener. In order to improve the performance of nanowire surface fastener, copper/parylene core/shell nanowire surface fastener was fabricated (Wang et al. 2013b). Compared with metallic nanowire surface fastener, the adhesion strength increased dramatically.

A peculiar cell (Fig. 6.4) was used to fabricate freestanding copper nanowire on the substrate directly. The introduced porous glass and porous cellulose membrane have three important functions. First, the capillary forces provided by the porous glass plate and the porous cellulose membrane help maintain a continuous electrolyte flow from the bulk of the electrolyte to PC membrane (Taberna et al. 2006). Second, the stiffness of porous glass plate ensures the contact of the substrate with PC membrane. Third, the compliance of the porous cellulose membrane offers a buffer and ensures a tight contact of the substrate with PC membrane. It is known that for flat anodes the metal is deposited preferentially at the outer border areas of the cathode (Wang et al. 2013b). This effect was avoided by using a conical copper anode, leading to a noticeably more homogeneous copper nanowire distribution

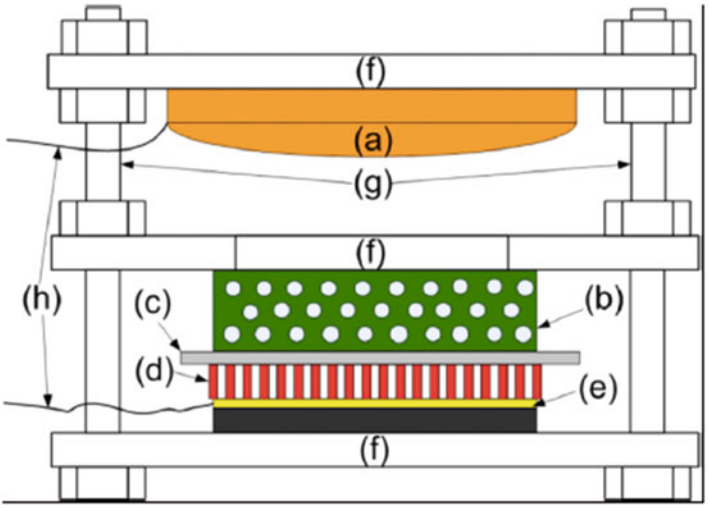

Fig. 6.4 Schematic of the cell for copper nanowire fabrication: (**a**) conical copper anode, (**b**) porous glass plate, (**c**) cellulose membrane, (**d**) polycarbonate template, (**e**) glass substrate with gold film, (**f**) isolation holder, (**g**) screw and nut, and (**h**) copper wire (Wang et al. 2013b)

over the whole cathode surface (Tomil et al. 2001). Before and after the assembly of the cell, two additional immersions were introduced to ensure an even copper ion density throughout the PC membrane (Millipore) (Wang et al. 2013b). Copper nanowire arrays were then synthesized by electrodeposition under a constant current. The electrodeposition electrolyte used was a 0.4 M $CuSO_4 \cdot 5H_2O$ solution, adjusted to pH 2 with sulfuric acid. The electrodeposition was performed at room temperature and without stir. After etching in methylene chloride to remove the PC membrane, the freestanding copper nanowire arrays on the substrate were obtained. Then, a thin film of Parylene C was deposited on copper nanowire arrays by using a DACS-LAB deposition system. The typical deposition conditions were 160 °C for the evaporation of the parylene dimer precursor, 650 °C for the pyrogenic decomposition of the dimer into monomers, and 60 mTorr for the vacuum chamber. Through controlling the amount of the loaded precursor, the corresponding thickness of parylene shell was obtained.

The fabrication procedure of the copper/parylene core/shell nanowire surface fastener is outlined in Fig. 6.5a. At first, copper nanowires were grown on glass/Cr/Au substrates by the template-assisted electrodeposition method. After etching the PC template, a thin layer of Parylene C was evenly deposited on the copper nanowires to enhance the adhesive ability of nanowire surface fastener. The SEM image of the copper nanowire arrays with an average diameter of 150 nm (Fig. 6.5b) indicates that most of the nanowires were grown vertically on the substrate, but oriented in a wide range of directions. Figure 6.5c, d show the SEM image of copper nanowires with a 100 and 200 nm parylene coating, respectively. Clearly, the grown copper nanowires sustain their high aspect ratio without aggregation, due to the high Young's modulus of the copper (110 GPa).

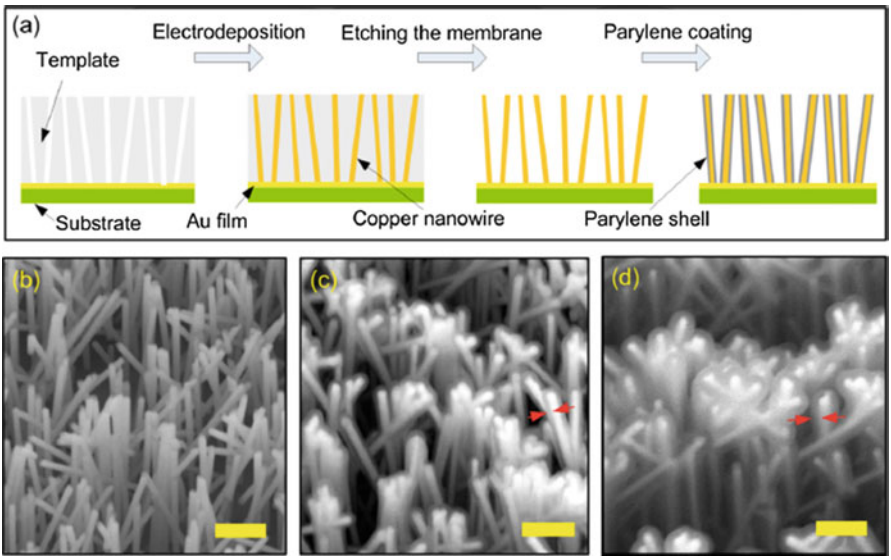

Fig. 6.5 (**a**) The fabrication process of copper/parylene core/shell nanowire. SEM images of copper nanowires (**b**) without parylene coating, (**c**) with 100 nm parylene coating, and (**d**) with 200 nm parylene coating. The *red arrows* in (**c**) and (**d**) indicate the parylene shell. The scale bar is 1 μm (Wang et al. 2013b)

6.4 Synthesis of Copper/Polystyrene Composite Nanowires

To further improve the performance of nanowire surface fastener, a copper/polystyrene core/shell nanowire surface fastener was prepared, which shows higher adhesion strength and a much lower electrical resistance than copper/parylene core/shell nanowire surface fastener (Wang et al. 2014, 2015).

The fabrication procedure of the copper/polystyrene core/shell nanowire surface fastener is shown in Fig. 6.6. The AAO membranes (Synkera Company) with a nominal pore diameter of ~80 nm and interpore distance of ~240 nm were used as templates for the synthesis of polystyrene nanotubes. These open-ended nanotubes were synthesized into the AAO template by spin-casting method (Jin et al. 2012; Wang et al. 2014). Briefly, a polymer solution (~20 μl of 2.5 wt% polystyrene solution in toluene) was directly loaded over the spinning AAO template. After 90 s of spinning, the toluene was evaporated and then the polystyrene nanotubes were formed in the template. The thickness of polystyrene nanotube can be controlled through adjusting the loaded times. After the formation of nanotubes, the copper nanowire array was fabricated into polystyrene nanotubes using template-assisted electrodeposition method (Wang et al. 2014) by setting up the stacked cell (Fig. 6.4) in a 0.4 M $CuSO_4 \cdot 5H_2O$ solution, under a constant current of 3 mA at room temperature. The pH value of the copper sulfate solution was maintained at pH 2

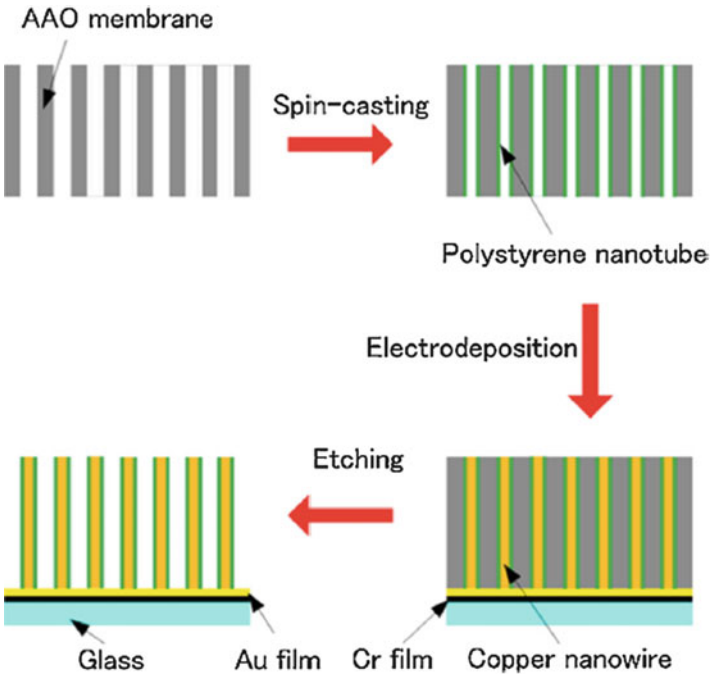

Fig. 6.6 Schematics of the fabrication process for the copper/polystyrene core/shell nanowire array (Wang et al. 2015)

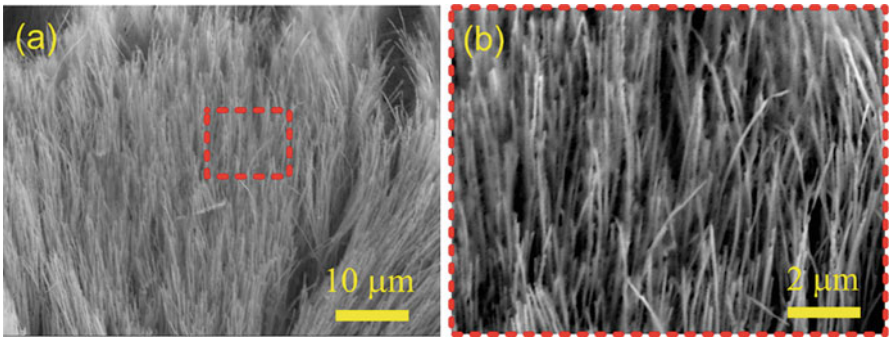

Fig. 6.7 SEM images of (**a**) a typical copper/polystyrene core/shell nanowire array and (**b**) enlarged view (Wang et al. 2015)

with sulfuric acid. Finally, the copper/polystyrene core/shell nanowire array was obtained after etching the AAO template by 3 M NaOH solution.

SEM image of a typical copper/polystyrene core/shell nanowire array is shown in Fig. 6.7, clearly indicating the mainly vertical orientation and the uniform shell thickness of the nanowires. Each of the components plays an essential role in

achieving the desired functionality of the electrical nanowire surface fasteners. The Cu core provides the following functions: (1) an electrical conductive function as the polymer shell shrinks to nanoscale (Wang et al. 2013b) and (2) preventing aggregation and/or collapse of nanowires, thereby resulting in high aspect ratio structures. The polystyrene shell enhances the surface compliance and the adhesion energy, thereby leading to an increase in the adhesion strength.

6.5 Fabrication of Carbon Nanotube Array

CNTs have been among the most scientifically studied materials for the past two decades (Gogotsi 2010). Due to their unique properties, such as extremely mechanical properties, high electrical conductivity, and thermal conductivity/stability (Chen et al. 2010; Cui et al. 2013a), CNTs have been suggested for a variety of practical applications (Cao and Rogers 2009; Cui and Zhang 2013a; Green et al. 2009; Wei and Liu 2008). The most intriguing properties of CNTs lie in their unique one-dimensional nanoscale structures that are anisotropic: properties in the longitudinal direction are drastically different from those in the azimuthal directions (Lan et al. 2011). It is highly desirable in the realization of most of the applications to control the orientation of CNTs either as a stand-alone system or in a group of many systems (Cui and Zhang 2013b).

CNT arrays typically comprise billions of CNTs per square centimeter. CNTs in a CNT array are nearly parallel to each other and have more uniform direction and length distribution than other kinds of CNTs such as tangled CNTs. CNT arrays can provide a well-defined large surface area, and they can be readily incorporated into devices with improved uniformities in mass production, greatly facilitating their integration into practical devices (Chen et al. 2010). Due to their highly ordered nature and high surface area with excellent electronic and mechanical properties (Liu et al. 2007), CNT arrays have wider applications than random bulk CNTs. These applications include field emission cathodes (Liao et al. 2010), supercapacitors (Niu et al. 1997), nanofiltration membranes (Dai 2002), and fuel cell and solar cells (Lan et al. 2011).

CNTs in CNT arrays are straight and uniformly aligned in the vertical direction, which is beneficial for fastener applications. Compared with metallic nanowires, CNTs are more bendable and have significant ability to entangle, both of which enhance side contact with fibrillary arrays. Moreover, CNTs possess good mechanical properties and high electrical conductivity, and are consequently predicted to have potential applications in electrical fasteners (Cui et al. 2014a). Therefore, CNT and Cu/parylene core/shell nanowire array was used to construct an electrical fastener. Compared with a metallic nanowire array fastener (Ju and Amano 2012; Wang et al. 2013a), the adhesion strength of the CNT-Cu/parylene nanowire array fastener is significantly greater, offering a sixfold increase that encourages their use in practical applications of room-temperature electrical fasteners (Cui et al. 2014a).

A Si wafer (<100> type, 1–10 Ω/cm) with a 600 nm SiO_2 layer was used as a substrate. A catalyst film of Fe (0.5–1.0 nm) was deposited on the Si wafer by electron beam (E-beam) evaporation (Edwards EB3 Electron Beam Evaporator). The evaporation was carried out at a pressure of about 5×10^{-7} Torr. The deposition rate of the Fe film was kept at 0.05 nm/s to achieve uniform and controllable film thickness. The thickness of the thin Fe film was monitored in situ by a quartz-crystal sensor fixed inside the E-beam evaporation chamber and calibrated ex situ by atomic force microscopy (AFM, Veeco Explorer).

The CNT arrays were synthesized in a quartz tube furnace. The reaction chamber was a quartz tube with a 3 in. diameter. The substrates were placed in the middle of the quartz tube and the quartz tube was pumped down to 5 mTorr to remove any ambient gas. The total pressure was maintained at 1 atm for all the experiments. The furnace was heated up to the growth temperature (690–780 °C) at 20 °C/min and under Ar flow. Then, C_2H_2 (99.99 %) and/or H_2 (99.99 %) were introduced into the reactor and the CNT arrays were synthesized at the growth temperature for a certain time. Lastly, the acetylene and/or hydrogen gas flow was turned off and the furnace was cooled down to room temperature with the Ar gas flow continuing (Cui et al. 2013a).

Figure 6.8 shows typical SEM images of CNT arrays on a Si substrate, grown under conditions of $C_2H_2 = 100$ sccm, $H_2 = 50$ sccm, and 750 °C. In the top layer of CNT array, it can be seen that the CNTs are entangled and not aligned (Fig. 6.8b).

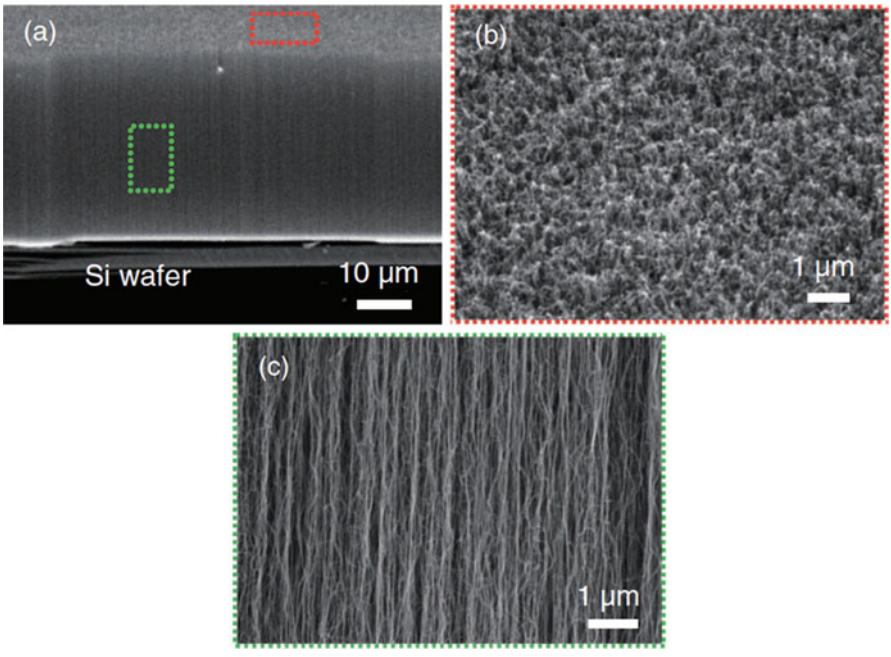

Fig. 6.8 (**a**) Cross-sectional SEM image of CNT array. (**b**) Top view of CNT array showing entanglement of CNTs at the surface. (**c**) High magnification SEM image showing the alignment of CNTs in the array side wall (Cui et al. 2014a)

It should be noted that the CNT array in this case was prepared by a normal chemical vapor deposition process, which can be easily scaled-up for the preparation of CNT arrays. The morphology of the top surface is similar to that of other CNT arrays prepared by low-pressure chemical vapor deposition methods (Qu et al. 2008). As shown in Fig. 6.8c, the CNTs in the array are well-aligned and bundled in the vertical direction, with these bundles being parallel to one another, while the waved CNTs switch between different straight CNT bundles. The curved CNTs in the top surface of the array, and the waved CNTs, can entangle and coil on the surface of Cu/parylene nanowires. This in turn increases the contact area between CNTs and Cu/parylene nanowires, which enhances the adhesion strength of the fastener (Cui et al. 2014a).

6.6 Mechanical and Electrical Performances of Nanowire Surface Fasteners

As shown in Fig. 6.9, a specific pattern for the fastener areas and printed wires (1 mm width) were designed to facilitate the testing of the mechanical bonding strength and the parasitic resistance of the electrical bonding. The diameter of each of the four fastener areas was 2 mm (Wang et al. 2013b). Au films approximately 100 nm thick were deposited onto the fastener and wire areas on Si or glass substrates with around 50 nm thick Cr adhesive layer to improve the adhesion between the substrate and the Au film. The adhesive layer and the Au film were deposited via E-beam evaporation or sputtering (Ju et al. 2012; Wang et al. 2015).

To better understand the adhesion performance of the nanowire surface fastener, we carried out macroscopic measurement of adhesion strength. The bonding strength is defined as the force acted to the nanowire surface fasteners to separate their bonding divided by the bonding area, in the normal and the shear directions. As shown in Fig. 6.10, two nanowire surface fastener samples (Fig. 6.10a), which had patterned nanowire arrays on the substrate, were brought into interconnection at a preload force (Fig. 6.10b) (Wang et al. 2013a). After the preload force was

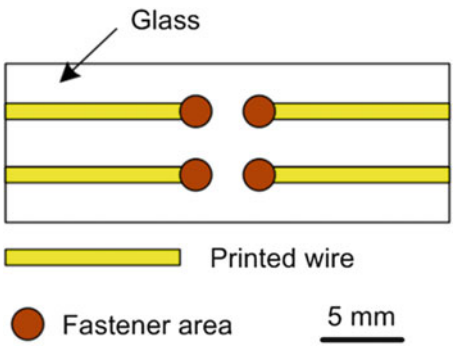

Fig. 6.9 Sketch of a sample with a specific pattern (Wang et al. 2014)

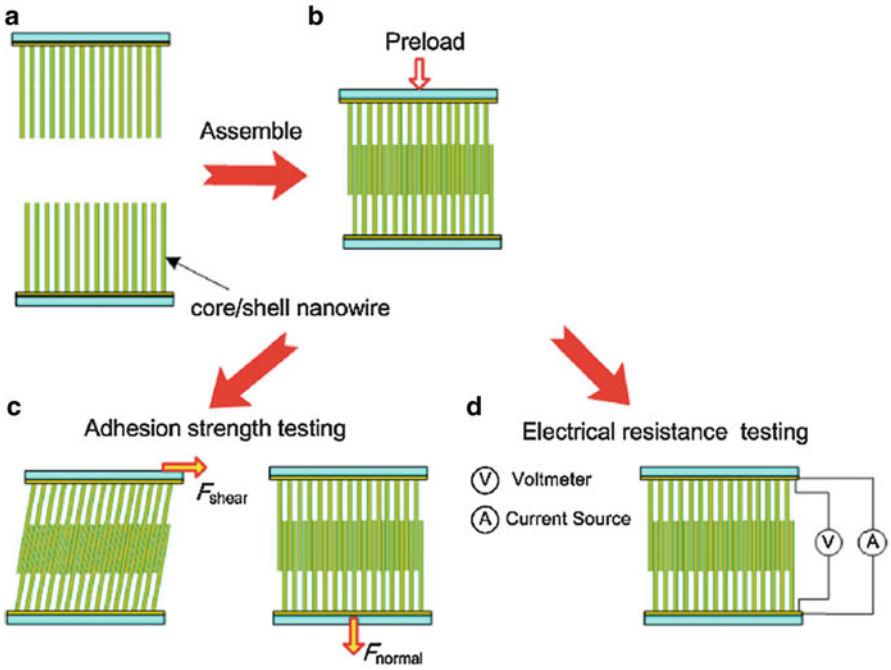

Fig. 6.10 The assembly sequence of patterned nanowire arrays as NSF together with the adhesion strength and electrical resistance test setup (Wang et al. 2015)

completely released, the weight of balance was used to measure the pull-off forces with the parallel (i.e., the shear adhesive strength) and normal (i.e., the normal adhesive strength) directions to the substrate (Fig. 6.10c) (Wang et al. 2015). To eliminate the effects of the attachment cycles and avoid the pre-alignment effect for subsequent adhesion measurements, the adhesion forces obtained from the first attachment of each sample were adopted. Adhesion tests for each reported condition were completed for four samples, and the average values were used. The four-point probe method was used to measure the electrical resistance (Fig. 6.10d). During the measurement, an electrical current in the range from 0 to 19 mA was applied using the current source and the corresponding voltage was extracted from the voltmeter (Wang et al. 2013b, 2015).

6.6.1 Performances of Copper/Parylene Nanowire Surface Fasteners

To characterize the properties of copper/parylene nanowire surface fasteners, we first measured the adhesive strength and relative electrical resistance as a function of nanowire length (5, 10, and 20 μm). All the samples in this test have a parylene

shell (100 nm thickness) and a preload of 78.02 N/cm^2. Interestingly, the Parylene C film becomes conductive due to dielectric breakdown when the thickness of it is miniaturized to nanoscale. The reason why Parylene C film in nanoscale thickness becomes conductive is mainly due to the dielectric breakdown phenomenon (Wang et al. 2013b). As can be seen in Fig. 6.11a, both shear and normal adhesion can be realized at the same time. Moreover, the adhesive strength is strongly affected by the length of the nanowires. The maximum shear and normal strengths were obtained when the length was 10 μm. When $L < 10$ μm, the nanowires sustained their high aspect ratio and the neighboring nanowires did not contact each other (Fig. 6.12a); therefore, the contact area is directly proportional to the nanowire length. However, when the nanowire length is as large as 20 μm, the nanowires tend to collapse and the neighboring nanowires contact each other (Fig. 6.12c), which leads to a reduction of the contact area of the nanowire surface fasteners. The electrical resistance is also strongly affected by the length of nanowires. Specifically, longer nanowire length results in a smaller electrical resistance (Fig. 6.11b). As can be seen in Fig. 6.12a–c, the interconnection of neighboring nanowires increases as the length of nanowires increases, and they were interconnected before the parylene coating. The interconnected neighboring nanowires connect in parallel in the electrical connection, which led to the reduction of resistance.

Besides the nanowire length, the adhesive strength and electrical resistance are also affected by the parylene thickness. The samples with the same nanowire length (10 μm) and the same preload (78.02 N/cm^2) are used in the test. As can be seen in Fig. 6.11c, the adhesive strength strongly depends on the thickness of the parylene shell. Specifically, weak adhesive strengths (~0.99 N/cm^2 in shear and ~0.57 N/cm^2 in normal directions) are obtained from the pristine copper nanowires. The adhesive strength is dramatically enhanced by the application of the parylene shell. When the thickness of the parylene shell is 150 nm, the maximum adhesive strengths (~24.97 N/cm^2 in shear and ~10.82 N/cm^2 in normal directions) are obtained. This significant enhancement in adhesion is attributed to the higher surface compliance of the parylene shell, enabling conformal contact with increased contact area between the interpenetrating nanowires (Kapadia et al. 2009). When the thickness of parylene shell further increases, the adhesive strengths decrease. This trend is attributed to the higher filling factor for thicker parylene shells (Fig. 6.5b–d). When the thickness of the parylene shell increases to 250 nm, almost no spare space exists between the neighboring nanowires (Wang et al. 2013b). Hence, the interconnected mode changes from "wire–wire" to "tip–tip" when the thickness of parylene shell increases, which results in the reduction of adhesive strengths. The electrical properties of nanowire surface fasteners are also affected by the parylene shell thickness. It can be seen from Fig. 6.11d that larger parylene shell thickness results in larger electrical resistance of the nanowire surface fasteners. This trend is attributed to the poor electrical conductivity of parylene. To examine the effect of preload on the adhesive and electrical properties of copper/parylene core/shell nanowire surface fastener, two nanowire surface fastener samples were brought into interconnection at a preload of 39.01, 78.02, and 156.04 N/cm^2. A monotonic increase in the normal adhesive strength and decrease in electrical resistance are

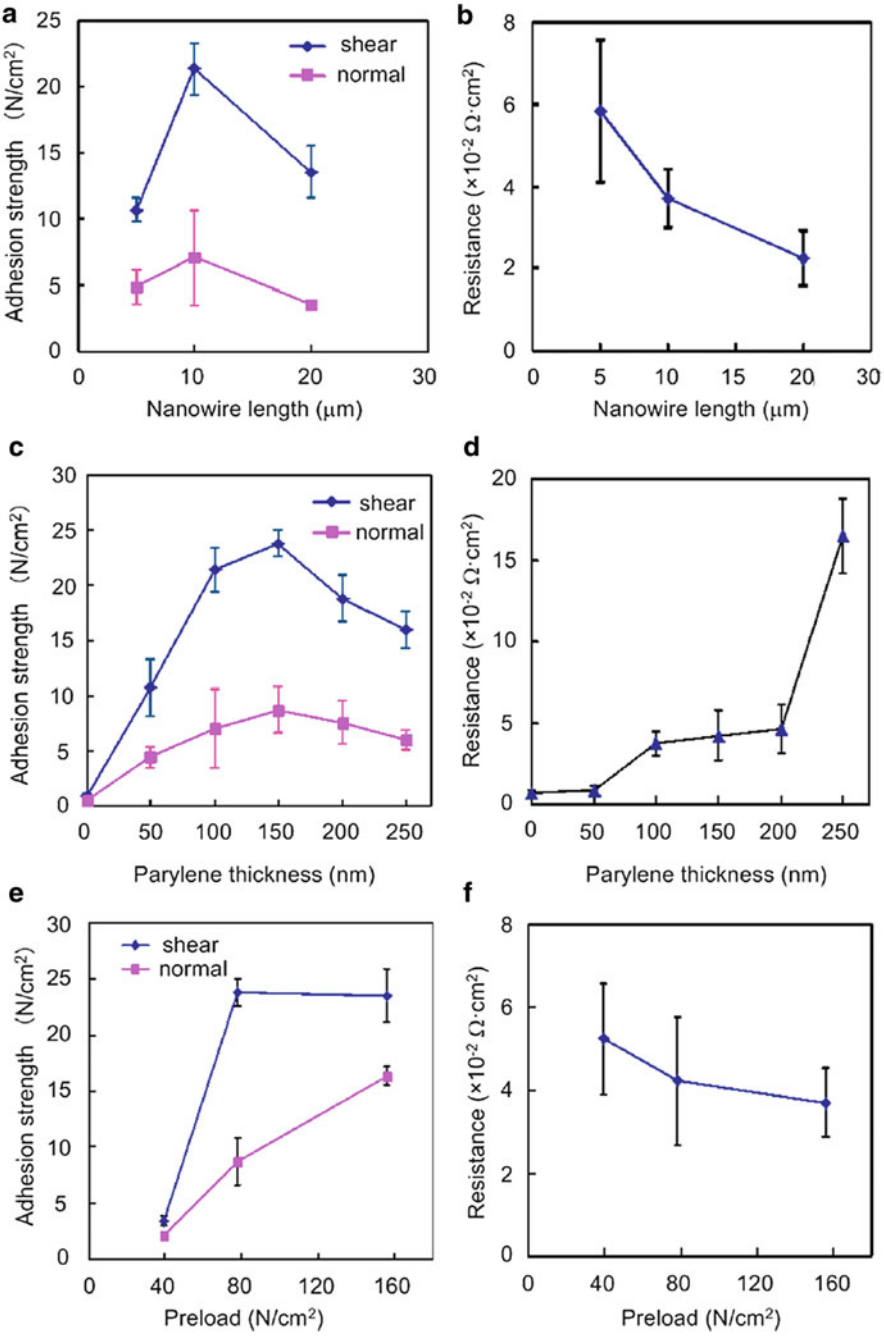

Fig. 6.11 (**a**) Adhesive strength and (**b**) electrical resistance of nanowire surface fasteners as a function of nanowire length. The preload is 78.02 N/cm^2 and the thickness of the parylene shell is 100 nm. (**c**) Adhesive strength and (**d**) electrical resistance of nanowire surface fasteners as a function of parylene thickness. The preload is 78.02 N/cm^2 and the length of the nanowire array is 10 μm. (**e**) Adhesive strength and (**f**) electrical resistance of nanowire surface fasteners as a function of preload. The thickness of parylene shell is 150 nm and the length of nanowire array is 10 μm (Wang et al. 2013b)

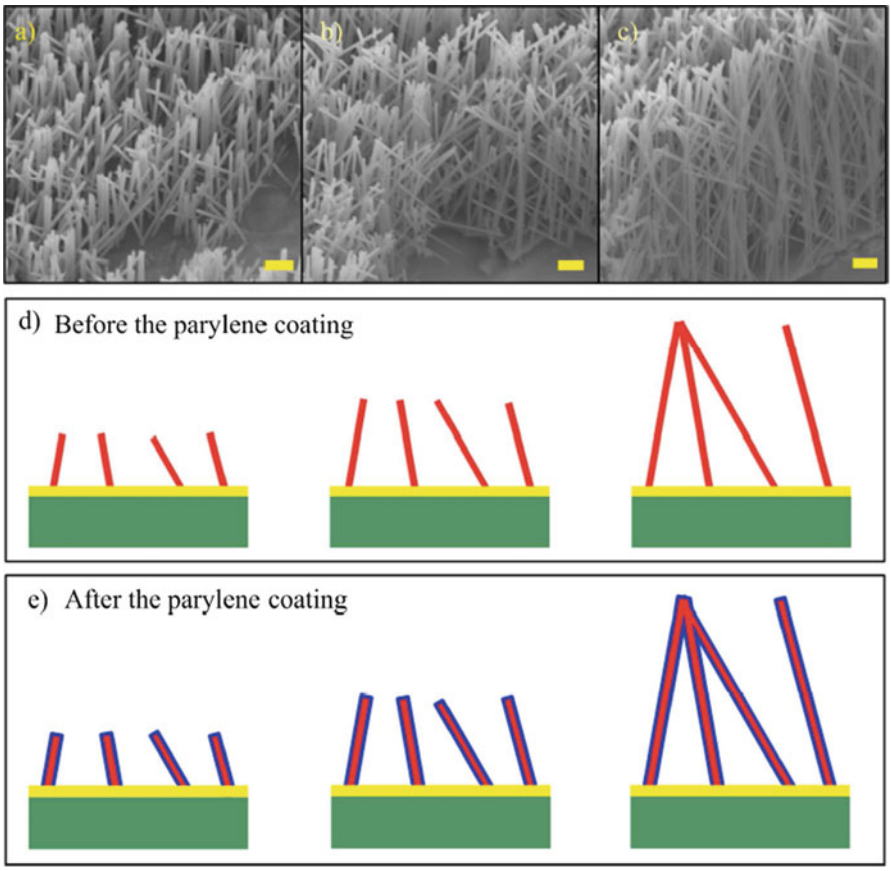

Fig. 6.12 (**a**–**c**) Side-view SEM images of copper nanowire arrays before parylene coating with lengths of 5, 10, and 20 μm. (**d**) Illustration of nanowire arrays before the parylene coating with the length of 5, 10, and 20 μm. (**e**) Illustration of nanowire arrays after the parylene coating with lengths of 5, 10, and 20 μm. The scale bar is 1 μm (Wang et al. 2013b)

observed with the increase of preload force (Fig. 6.11e, f). This phenomenon is just as expected because the higher preload force leads to a larger contact area between the nanowires. However, no increase in the shear adhesion was observed when the preload increases from 78.02 to 156.04 N/cm^2. This phenomenon is attributed to the poor adhesion of electrodeposited copper nanowires on the Au seed layer (Wang et al. 2013b).

Figure 6.13a shows a schematic of copper/parylene core/shell nanowire surface fasteners. An example of the strong bonding achieved is shown in Fig. 6.13b in which the copper/parylene core/shell nanowire surface fasteners with a surface area of ~3.14×4 mm^2 enables 300 g of weight to be hung without failure in the shear direction. As shown in Fig. 6.13c, the red light from the light-emitting diode shows that the core/shell nanowire surface fasteners are conductive.

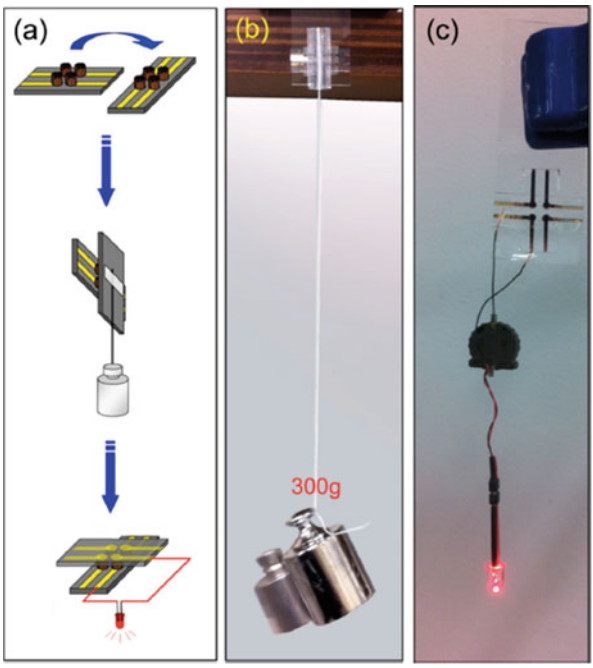

Fig. 6.13 (**a**) Schematic of this room-temperature electrical bonding technique. (**b**) Photo showing a weight of 300 g hanging on the interconnected copper nanowire surface fasteners. (**c**) Light-emitting diode suspended by the nanowire surface fasteners to show electrical conductivity (Wang et al. 2013b)

6.6.2 *Performances of Copper/Polystyrene Nanowire Surface Fasteners*

To demonstrate the importance of the polystyrene shell, we systematically studied the adhesion strength as a function of polystyrene thickness. The samples with the same nanowire length (40 μm) and the same preload (9.8 N) are used in the test. As can be seen in Fig. 6.14a, the adhesive properties strongly depend on the thickness of the polystyrene shell. Specifically, weak adhesion strengths (1.25 N/cm^2 in shear and 0.76 N/cm^2 in normal directions) are obtained from the pristine copper nanowires. The adhesion strength is dramatically enhanced by the application of polystyrene shell. When the thickness of the polystyrene shell is 18 nm, the maximum adhesion strengths (44.42 N/cm^2 in shear and 21.43 N/cm^2 in normal) are obtained. This drastic enhancement of the adhesion strength with polystyrene shell thickness can be explained by an increase in contact width between the engaged nanowire arrays (Kapadia et al. 2009). A decrease in adhesion strength is observed for the thickness of the polystyrene shell that is larger than 18 nm. This trend is attributed to decrease the density of Cu core because of thicker polystyrene shells. When the thickness of the polystyrene shell increases to 24 nm, the polystyrene nanotube becomes more hydrophobic which prevents the electrolyte getting into the polystyrene nanotube and then decreasing the density of Cu core (Jin et al. 2005). The electrical properties of copper/polystyrene core/shell nanowire

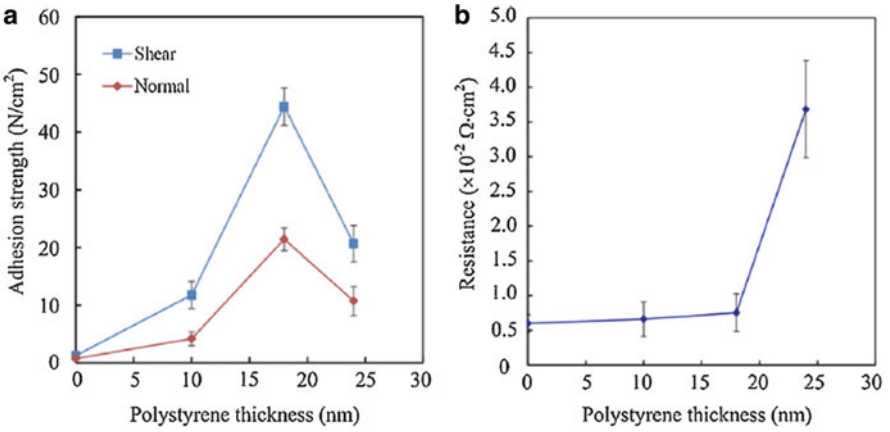

Fig. 6.14 (**a**) Adhesion strength and (**b**) electrical resistance of nanowire surface fastener as a function of polystyrene thickness. The preload is 9.8 N and the length of nanowire array is ~40 μm (Wang et al. 2015)

surface fastener are also affected by the polystyrene shell thickness. It can be seen from Fig. 6.14b that larger polystyrene shell thickness results in larger electrical resistance of the nanowire surface fastener. This trend is attributed to the poor electrical conductivity of polystyrene (Wang et al. 2015).

Besides the polystyrene shell thickness, the adhesion strength is also affected by the molecular weight of polystyrene shell. The samples with the same shell thickness (18 nm) and the same preload (9.8 N) are used in the test. As can be seen in Fig. 6.15a, a monotonic increase in the adhesion strength is observed with the molecular weight of polystyrene. Specifically, the shear adhesion strength increases from 4.64 to 44.42 N/cm^2 as the molecular weight of polystyrene is increased from 35,000 to 350,000 g/mol. The adhesion energy of polystyrene increases with an increase in the molecular weight, thus enhancing the adhesion forces between the core/shell nanowires (Lau and Burns 1974). On the other hand, the changes of the electrical resistance for the nanowire surface fastener were rather small when the molecular weight of polystyrene varied (Fig. 6.15b). The reason is due to that polystyrene shells reach dielectric breakdown and become conductive at this thickness, which is no relationship with the molecular weight of polystyrene shells (Wang et al. 2015).

Compared with the copper/parylene core/shell nanowire surface fastener (Wang et al. 2013b), the copper/polystyrene core/shell nanowire surface fastener tends to achieve higher adhesion strength. Different with parylene, polystyrene is a kind of solvent-welding plastic. Plastic solvent-welding is a technique which uses a solvent to partially liquefy plastic along the joint and allows the joint to solidify, causing a permanent chemical weld. Besides the van der Waals force, the chemical force has a big contribution to the adhesion strength. That is the reason that polystyrene shell has a better performance than parylene shell for nanowire surface fastener. Moreover, the polymer shell thickness of copper/polystyrene core/shell nanowire surface

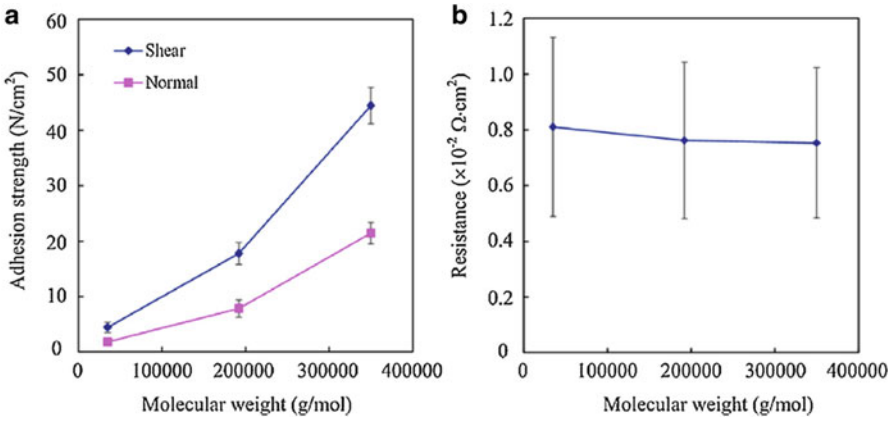

Fig. 6.15 (**a**) Adhesion strength and (**b**) electrical resistance of nanowire surface fastener as a function of the molecular weight of polystyrene. The preload is 9.8 N and the thickness of polystyrene shell is ~18 nm (Wang et al. 2015)

fastener is much thinner than that of copper/parylene core/shell nanowire surface fastener (Wang et al. 2013b), which leads to a good electrical conductivity of copper/polystyrene core/shell nanowire surface fastener. On the other hand, the copper/polystyrene core/shell nanowire surface fastener was fabricated by synthesizing copper nanowires into polystyrene nanotubes, which may easily form homogeneous polymer shell along the whole length of copper nanowires by comparing with copper/parylene core/shell nanowire surface fastener which was formed by coating parylene shell on core copper nanowires (Wang et al. 2015).

6.6.3 *Performances of CNT-Copper/Parylene Nanowire Surface Fasteners*

To characterize the performance of a CNT-Cu/parylene nanowire array fastener, we systematically measured the macroscopic shear and normal adhesion strength as a function of the CNT array length (Fig. 6.16a). This revealed that the adhesion strength of a CNT-Cu/parylene nanowire array fastener steadily increases with the increase in the length of the CNT array. For example, the adhesive shear strength increases almost linearly from 20.29 to 50.72 N/cm^2 when the length of the CNT array increases from 35 to 120 μm. The maximum adhesive shear strength obtained of 50.72 N/cm^2 is comparable to that achievable with CNT-based adhesives (Qu et al. 2008; Qu and Dai 2007) and is six times higher than that of a metallic nanowire fastener (Ju et al. 2012; Ko et al. 2009; Wang et al. 2013a). The corresponding normal adhesion strength also increases from 14.82 to 28.48 N/cm^2 over the same range of CNT lengths, which is approximately five times higher than that of a metallic nanowire fastener (Ju et al. 2012; Wang et al. 2013a). Unlike

gecko adhesives, the CNT-Cu/parylene nanowire array fastener produces both high shear and normal adhesion strengths simultaneously, which is important for the practical application of electrical fasteners.

Besides the length of the CNT array, the adhesion strength of CNT-Cu/parylene nanowire array fasteners is also affected by the preload applied to engage the fastener. As shown in Fig. 6.16b, the adhesion strength of a CNT-Cu/parylene nanowire array fastener increases with the applied preload. Specifically, it increases from 7.02 to 20.29 N/cm^2 as the preload is increased from 4.9 to 19.6 N. The interpenetration depth between CNTs and Cu/parylene nanowires increases with an increase in the applied preload force, thus enhancing the contact area and van der Waals interactions between the CNTs and Cu/parylene nanowires (Hyunhyub et al. 2010; Chen et al. 2012).

As shown in Fig. 6.17a, the electrical resistance of the CNT-Cu/parylene nanowire array fastener was investigated. The solid lines in the figure are obtained through linear fitting of the measured values. The resistance of the fastener was extracted from the *I*–*V* curves (Fig. 6.17b) (Kapadia et al. 2009). As shown in Fig. 6.17a, the fastener exhibits ohmic behavior over the entire range of measurement; however, the resistance of the fastener decreases with an increase in the preload force. For example, the resistance decreases from 142.3 to 45.4 Ω when the preload force is increased from 0 to 19.6 N as shown in Fig. 6.17b, which indicates that the CNT-Cu/parylene nanowire array fastener has good electrical conductivity. Since an increase in preload force increases the interpenetration depth and connection between CNTs and Cu/parylene nanowires, the electrical performance of the fastener is also improved (Cui et al. 2014a). It should also be noted that the resistance of the CNT-Cu/parylene nanowire array fastener was almost constant for the first 20 cycles of attachment–detachment tests.

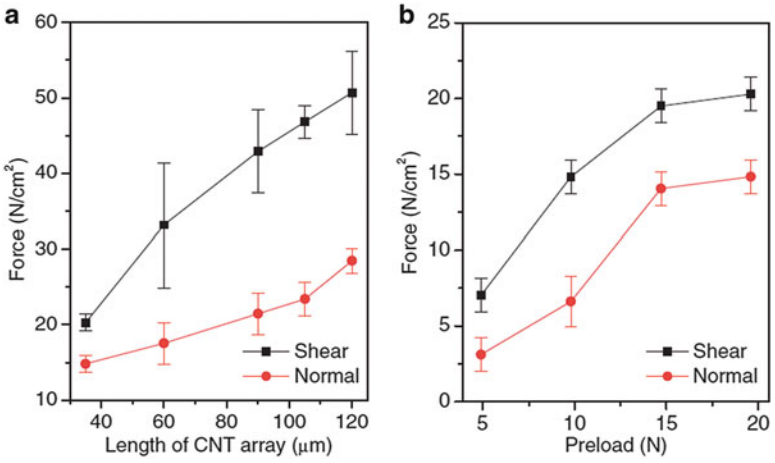

Fig. 6.16 (**a**) Shear and normal adhesion force of a CNT-Cu/parylene nanowire array fastener as a function of the CNT array length. The preload used to engage the fastener was 19.6 N. (**b**) Preload force-dependent adhesion force of a CNT-Cu/parylene nanowire array fastener. The errors represent standard errors calculated from four measurements (Cui et al. 2014a)

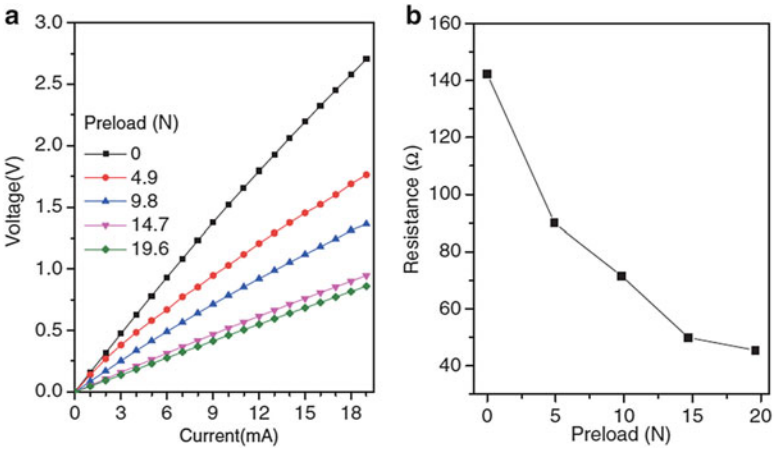

Fig. 6.17 (**a**) *I–V* curves of CNT-Cu/parylene array fastener under different preload forces. (**b**) Measured resistance as a function of preload force (Cui et al. 2014a)

6.7 Conclusions

In this chapter, we outlined the progress made in the use of composite nanowires for room-temperature mechanical and electrical bonding. The fabrication of Cu/parylene and Cu/polystyrene nanowires using AAO and PC membrane as templates was described. While, the fabrication of carbon nanotube (CNTs) array used to connect with Cu/parylene nanowires was also discussed. For copper/parylene core/shell nanowire array, both strong bonding and small electrical resistance were achieved at room temperature. It is important to note that this electrical surface fastener exhibits high macroscopic adhesion strength (25 N/cm^2) and low electrical resistance (4.22×10^{-2} Ω cm^2). We also developed an electrical surface fastener with strong adhesion based on copper/polystyrene core/shell nanowire arrays. The adhesion strength of this surface fastener could be mediated by the shell thickness and the molecular weight of polystyrene. Uniquely, this electrical surface fastener exhibits high macroscopic adhesion strength (44.42 N/cm^2) and low electrical resistance (~0.75×10^{-2} Ω cm^2), indicative that the copper/polystyrene core/shell nanowire surface fastener exhibits a higher adhesion strength and a lower electrical resistance than the copper/parylene core/shell nanowire surface fastener. Besides, copper/parylene nanowires and a CNT array were also chosen to construct a room-temperature electrical fastener. The adhesion strength of this fastener was found to increase with an increase in the length of the CNT arrays. The shear adhesion strength (50.72 N/cm^2) of the CNT-Cu/parylene nanowire array fastener is shown to be six times higher than that of a metallic nanowire fastener. The resistance of the fastener was measured as 45.4 Ω, which indicates that it has good electrical conductivity. In comparison with conventional reflow soldering method, the present cold bonding technique can be performed at room temperature,

which could improve the process compatibility and component reliability. Furthermore, a type of surface fastener without solder enables easier detachment of the surface mount component from the circuit board, by which recycling and sustainability of rare metals becomes significantly more convenient.

References

Attaluri, A.C., Huang, Z., Belwalkar, A., Van, G.W., Gao, D., Misiolek, W.: Evaluation of nanoporous alumina membranes for hemodialysis application. ASAIO J. **55**, 217–223 (2009)

Baek, S.S., Fearing, R.S.: Reducing contact resistance using compliant nickel nanowire arrays. IEEE T. Compon. Pack. T. **31**, 859–868 (2009)

Bakshi, M.S., Poonam, S., Banipal, T.S.: Au and Au-Ag bimetallic nanoparticles synthesized by using 12-3-12 cationic Gemini surfactant as template. Mater. Lett. **61**, 5004–5009 (2007)

Belwalkar, A., Grasing, E., Geertruyden, W.V., Huang, Z., Misiolek, W.Z.: Effect of processing parameters on pore structure and thickness of anodic aluminum oxide (AAO) tubular membranes. J. Memb Sci. **319**, 192–198 (2008)

Cao, Q., Rogers, J.A.: Ultrathin films of single-walled carbon nanotubes for electronics and sensors: a review of fundamental and applied. Adv. Mater. **21**, 29–53 (2009)

Chen, B., Goldberg Oppenheimer, P., Shean, T.A.V., Wirth, C.T., Hofmann, S., Robertson, J.: Adhesive properties of gecko-inspired mimetic via micropatterned carbon nanotube forests. J. Phys. Chem. C **116**, 20047–20053 (2012)

Chen, H., Roy, A., Baek, J.B., Zhu, L., Qu, J., Dai, L.: Controlled growth and modification of vertically-aligned carbon nanotubes for multifunctional applications. Mat. Sci. Eng. R. **70**, 63–91 (2010)

Chen, P.L., Kuo, C.T., Tsai, T.G., Wu, B.W., Hsu, C.C., Pan, F.M.: Self-organized titanium oxide nanodot arrays by electrochemical anodization. Appl. Phys. Lett. **83**, 2796–2798 (2003)

Chung, C.K., Chang, W.T., Liao, M.W., Chang, H.C., Lee, C.T.: Fabrication of enhanced anodic aluminum oxide performance at room temperatures using hybrid pulse anodization with effective cooling. Electrochim Acta **56**, 6489–6497 (2011)

Chung, C.K., Liao, M.W., Khor, O.K.: Fabrication of porous anodic aluminum oxide by hybrid pulse anodization at relatively high potential. Microsyst. Technol. **20**, 1827–1832 (2013)

Chu, S.Z., Todoroki, S., Wada, K., Inoue, S.: Formation and microstructures of anodic alumina films from aluminum sputtered on glass substrate. J. Electrochem. Soc. **149**, B321–B327 (2001)

Chu, S.Z., Wada, K., Inoue, S., Isogai, M., Yasumori, A.: Fabrication of ideally ordered nanoporous alumina films and integrated alumina nanotubule arrays by high-field anodization. Adv. Mater. **17**, 2115–2119 (2005)

Crouse, D., Lo, Y.H., Miller, A.E., Crouse, M.: Self-ordered pore structure of anodized aluminum on silicon and pattern transfer. Appl. Phys. Lett. **76**, 49–51 (2000)

Cui, J., Wu, Y., Wang, Y., Zheng, H., Xu, G., Zhang, X.: A facile and efficient approach for pore-opening detection of anodic aluminum oxide membranes. Appl. Surf. Sci. **258**, 5305–5311 (2012)

Cui, Y., Ju, Y., Wang, P., Xu, B., Kojima, N., Ichioka, K., Hosoi, A.: Carbon nanotube–Cu/parylene nanowire array electrical fasteners with high adhesion strength. Appl. Phys. Express **7**, 015012 (2014a)

Cui, Y., Ju, Y., Xu, B., Wang, P., Kojima, N., Ichioka, K., Hosoi, A.: Mimicking a gecko's foot with strong adhesive strength based on a spinnable vertically aligned carbon nanotube array. RSC Adv. **4**, 9056 (2014b)

Cui, Y., Wang, B., Zhang, M.: Optimizing reaction condition for synthesizing spinnable carbon nanotube arrays by chemical vapor deposition. J. Mater. Sci. **48**, 7749–7756 (2013)

Cui, Y., Zhang, M.: Cross-links in carbon nanotube assembly introduced by using polyacrylonitrile as precursor. ACS Appl. Mater. Inter. **16**, 8173–8178 (2013a)

Cui, Y., Zhang, M.: Fabrication of cross-linked carbon nanotube foam using polymethylmethacrylate microspheres as templates. J. Mater. Chem. **1**, 13984–13988 (2013b)

Dai, H.: Carbon nanotubes: synthesis, integration, and properties. Acc. Chem. Res. **35**, 1035–1044 (2002)

Demoustier, S.: Preparation of polymeric and metallic nanostructures using a template-based deposition method. Mater. Sci. Eng. C **15**, 269–271 (2001)

Ding, G.Q., Shen, W.Z., Zheng, M.J., Fan, D.H.: Synthesis of ordered large-scale ZnO nanopore arrays. Appl. Phys. Lett. **88**, 103106 (2006)

Dong, L., Tao, X., Zhang, L., Zhang, X., Nelson, B.J.: Nanorobotic spot welding: controlled metal deposition with attogram precision from copper-filled carbon nanotubes. Nano Lett. **7**, 58–63 (2006)

Feng, X., Hangarter, C., Yoo, B., Rheem, Y., Lee, K.H., Myung, N.V.: Recent progress in electrodeposition of thermoelectric thin films and nanostructures. Electrochim. Acta **53**, 8103–8117 (2008)

Ferguson, G.S., Chaudhury, M.K., Sigal, G.B., Whitesides, G.M.: Contact adhesion of thin gold films on elastomeric supports: cold welding under ambient conditions. Science **253**, 776–778 (1991)

Gâlcă, A.C., Kooij, E.S., Wormeester, S., Salm, C., Leca, V., Rector, J.H., Poelsema, B.: Structural and optical characterization of porous anodic aluminum oxide. J. Appl. Phys. **94**, 4296–4305 (2003)

Gogotsi, Y.: High-temperature rubber made from carbon nanotubes. Science **330**, 1332–1333 (2010)

Gorokh, G., Mozalev, A., Solovei, D., Khatko, V., Llobet, E., Correig, X.: Anodic formation of low-aspect-ratio porous alumina films for metal-oxide sensor application. Electrochim. Acta **52**, 1771–1780 (2006)

Green, M.J., Behabtu, N., Pasquali, M., Adams, W.W.: Nanotubes as polymers. Polymer **50**, 4979–4997 (2009)

Harman, T.C., Taylor, P.J., Spears, D.L., Walsh, M.P.: Thermoelectric quantum-dot superlattices with high ZT. J. Electron. Mater. **29**, L1–L2 (1999)

Huczko, A.: Template-based synthesis of nanomaterials. Appl. Phys. A **70**, 365–376 (2000)

Hyunhyub, K., Zhang, Z., Ho, J.C., Kuniharu, T., Rehan, K., Yu-Lun, C., Weizhen, C., Brett, A.C., Ali, J.: Flexible carbon-nanofiber connectors with anisotropic adhesion properties. Small **6**, 22–26 (2010)

Jin, C., Suenaga, K., Iijima, S.: Plumbing carbon nanotubes. Nat. Nanotechnol. **7**, 17–21 (2008)

Jin, M., Feng, X., Feng, L., Sun, T., Zhai, J., Li, T., Jiang, L.: Superhydrophobic aligned polystyrene nanotube films with high adhesive force. Adv. Mater. **17**, 1977–1981 (2005)

Jin, S., Lee, Y., Jeon, S.M., Sohn, B.H., Chae, W.S., Lee, J.K.: Simple fabrication of single-and multi-layer polymer nanotubes by spin-casting method within anodized aluminum oxide (AAO) templates. J. Mater. Chem. **22**, 23368–23373 (2012)

Joo, S.W., Banerjee, A.N.: FESEM studies of densely packed aligned nickel nanopillars on silicon substrate by electrochemical deposition through porous alumina membrane. Mater. Sci. Eng. B **175**, 36–40 (2010)

Ju, Y., Amano, M., Chen, M.: Mechanical and electrical cold bonding based on metallic nanowire surface fasteners. Nanotechnology **23**, 365202 (2012)

Kasi, A.K., Kasi, J.K., Afzulpurkar, N., Bohez, E., Tuantranont, A.: Continuous Voltage Detachment and Etching (CVDE) technique for fabrication of nano-porous anodic aluminum oxide (AAO) tubular membrane. Nanosci. Nanotech. Lett. **4**, 530–536 (2012)

Kapadia, R., Ko, H., Chueh, Y.L., Ho, J.C.: Hybrid core-multishell nanowire forests for electrical connector applications. Appl. Phys. Lett. **94**, 263110 (2009)

Kim, B., Park, S., McCarthy, T.J., Russell, T.P.: Fabrication of ordered anodic aluminum oxide using a solvent-induced array of block-copolymer micelles. Small **3**, 1869–1872 (2007)

Ko, H., Lee, J., Schubert, B.E., Chueh, Y.L., Leu, P.W., Fearing, R.S., Javey, A.: Hybrid core-shell nanowire forests as self-selective chemical connectors. Nano Lett. **9**, 2054–2058 (2009)

Lan, Y., Wang, Y., Ren, Z.F.: Physics and applications of aligned carbon nanotubes. Adv. Phys. **60**, 553–678 (2011)

Lau, W.W.Y., Burns, C.M.: Effect of temperature and molecular weight on the rate of spreading of polystyrene melts on plane soda lime glass surfaces. J. Polym. Sci. Pol. Phys. **12**, 431–439 (1974)

Liao, Q., Yang, Y., Qi, J., Zhang, Y., Huang, Y., Xia, L., Liu, L.: High intensity, plasma-induced electron emission from large area carbon nanotube array cathodes. Appl. Phys. Lett. **96**, 073109 (2010)

Li, D., Wu, Y., Fan, R., Yang, P., Majumdar, A.: Thermal conductivity of Si/SiGe superlattice nanowires. Appl. Phys. Lett. **83**, 3186–3188 (2003)

Li, H., Xu, C.L., Zhao, G.Y., Li, H.L.: Effects of annealing temperature on magnetic property and structure of amorphous Co49Pt51 alloy nanowire arrays prepared by direct-current electrodeposition. J. Phys. Chem. B **109**, 3759–3763 (2005)

Liu, K., Jiang, K., Wei, Y., Ge, S., Liu, P., Fan, S.: Controlled termination of the growth of vertically aligned carbon nanotube arrays. Adv. Mater. **19**, 975–978 (2007)

Li, Y., Wang, J., Deng, Z., Wu, Y., Sun, X., Yu, D., Yang, D.: Bismuth nanotubes: a rational low-temperature synthetic route. J. Am. Chem. Soc. **123**, 9904–9905 (2001)

Mao, R.W., Lin, S.K., Tsai, C.S.: In situ preparation of an ultra-thin nanomask on a silicon wafer. Nanotechnology **20**, 685–688 (2009)

Masuda, H., Fukuda, K.: Ordered metal nanohole arrays made by a two-step replication of honeycomb structures of anodic alumina. Science **268**, 1466–1468 (1995)

Niu, C., Sichel, E.K., Hoch, R., Moy, D., Tennent, H.: High power electrochemical capacitors based on carbon nanotube electrodes. Appl. Phys. Lett. **70**, 1480–1482 (1997)

Pastore, I., Poplausks, R., Apsite, I., Pastare, I., Lombardi, F., Erts, D.: Fabrication of ultra thin anodic aluminium oxide membranes by low anodization voltages. IOP Conf. Ser. Mater. Sci. Eng. **23**, 012025 (2011)

Peng, Y., Cullis, Y., Inkson, B.: Bottom-up nanoconstruction by the welding of individual metallic nanoobjects using nanoscale solder. Nano Lett. **9**, 91–96 (2008)

Pu, L., Shi, Y., Zhu, J.M., Bao, X.M., Zhang, R., Zheng, Y.D.: Electrochemical lithography: fabrication of nanoscale Si tips by porous anodization of Al/Si wafer. Chem. Commun. **8**, 942–943 (2004)

Qu, L., Dai, L.: Gecko-foot-mimetic aligned single-walled carbon nanotube dry adhesives with unique electrical and thermal properties. Adv. Mater. **19**, 3844–3849 (2007)

Qu, L., Dai, L., Stone, M., Xia, Z., Wang, Z.L.: Carbon nanotube arrays with strong shear binding-on and easy normal lifting-off. Science **322**, 238–242 (2008)

Sumikura, S., Mori, S., Shimizu, S., Usami, H., Suzuki, E.: Syntheses of NiO nanoporous films using nonionic triblock co-polymer templates and their application to photo-cathodes of p-type dye-sensitized solar cells. J. Photochem. Photobiol. A Chem **199**, 1–7 (2008)

Taberna, P.L., Mitra, S., Poizot, P., Simon, P., J-M, T.: High rate capabilities Fe_3O_4-based Cu nano-architectured electrodes for lithium-ion battery applications. Nat. Mater. **5**, 567–573 (2006)

Teshima, H., Kojima, K., Ju, Y.: Fabrication of anodic aluminum oxide template and copper nanowire surface fastener. J. Electron. Packaging **136**, 044501 (2014)

Tomil, M.M.E., Buschmann, V., Dobrev, D., Neumann, R., Scholz, R., Schuchert, I.U., Vetter, J.: Single-crystalline copper nanowires produced by electrochemical deposition in polymeric ion track membranes. Adv. Mater. **13**, 62–65 (2001)

Venkatasubramanian, R., Siivola, E., Colpitts, T., O'Quinn, B.: Thin-film thermoelectric devices with high room-temperature figures of merit. Nature **413**, 597–602 (2001)

Wang, P., Ju, Y., Chen, M., Hosoi, A., Song, Y., Iwasaki, Y.: Room-temperature bonding technique based on copper nanowire surface fastener. Appl. Phys. Express **6**, 035001 (2013a)

Wang, P., Ju, Y., Cui, Y., Hosoi, A.: Copper/parylene core/shell nanowire surface fastener used for room-temperature electrical bonding. Langmuir **29**, 13909–13916 (2013b)

Wang, P., Ju, Y., Hosoi, A.: Core-shell nanowire based electrical surface fastener used for room-temperature electronic packaging bonding. Electron. Mater. Lett. **10**, 503–507 (2014)

Wang, P., Ju, Y., Chen, M.: Room-temperature electrical bonding technique based on copper/polystyrene core/shell nanowire surface fastener. Appl. Surf. Sci. **349**, 774–779 (2015)

Wei, D., Liu, Y.: The intramolecular junctions of carbon nanotubes. Adv. Mater. **20**, 2815–2841 (2008)

Wei, S., Shen, Y., Ge, D., Xue, M., Cao, H., Huang, S., Wang, J.X., Zhang, G.L., Zhang, F.B.: Functionalized anodic aluminum oxide (AAO) membranes for affinity protein separation. J. Membr. Sci. **325**, 801–808 (2008)

Wei, W.X., Guang, T.F., Jinm, X.X., Zhen, J., De, Z.L.: Size-dependent orientation growth of large-area ordered Ni nanowire arrays. J. Phys. Chem. B **109**, 24326 (2005)

Woo, L., Roland, S., Kornelius, N., Ulrich, G.S.: A template-based electrochemical method for the synthesis of multisegmented metallic nanotubes. Angew. Chem. Int. Ed. Engl. **44**, 6050–6054 (2005)

Xu, J., Cheng, G., Zheng, R.: Controllable synthesis of highly ordered Ag nanorod arrays by chemical deposition method. Appl. Surf. Sci. **256**, 5006–5010 (2010)

Xu, J., Razeeb, K. M., Sitaraman, S. K., Mathewson, A.: The fabrication of ultra long metal nanowire bumps and their application as interconnects. Nanotechnology. IEEE C Nano 12th, pp. 1–6 (2012)

Yan, B., Pham, H.T.M., Ma, Y., Zhuang, Y., Sarro, P.M.: Fabrication of in situ ultrathin anodic aluminum oxide layers for nanostructuring on silicon substrate. Appl. Phys. Lett. **91**, 053117 (2007)

Zaraska, L., Sulka, G.D., Jaskula, M.: Anodic alumina membranes with defined pore diameters and thicknesses obtained by adjusting the anodizing duration and pore opening/widening time. J. Solid State Electr. **15**, 2427–2436 (2011)

Zhiyong, F., Haleh, R., Jae-won, D., Aimee, M., Onur, E., Yu-Lun, C., Paul, W.L., Johnny, C.H., Toshitake, T., Lothar, A.R., Steven, N., Kyoungsik, Y., Ming, W., Joel, W.A., Ali, J.: Three-dimensional nanopillar-array photovoltaics on low-cost and flexible substrates. Nat. Mater. **8**, 648–653 (2009)